Published in final edited form as:
Nano Lett. 2012 July 11; 12(7): 3391–3398. doi:10.1021/nl3015632.

Gold Nanoparticles for Neural Prosthetics Devices

Huanan Zhang[1], **Jimmy Shih**[1], **Jian Zhu**[1], and **Nicholas A. Kotov**[1,*]
[1]Department of Chemical Engineering, University of Michigan, Ann Arbor, Michigan, 48109

Abstract

Treatments of neurological diseases and the realization of brain-computer interfaces require ultrasmall electrodes which are “invisible” to resident immune cells. Functional electrodes smaller than 50μm are impossible to produce with traditional materials due to high interfacial impedance at the characteristic frequency of neural activity and insufficient charge storage capacity. The problem can be resolved by using gold nanoparticle nanocomposites. Careful comparison indicates that layer-by-layer assembled films from Au NPs provide more than threefold improvement in interfacial impedance and one order of magnitude increase in charge storage capacity. Prototypes of microelectrodes could be made using traditional photolithography. Integration of unique nanocomposite materials with microfabrication techniques opens the door for practical realization of the ultrasmall implantable electrodes. Further improvement of electrical properties is expected when using special shapes of gold nanoparticles.

Keywords

Au nanoparticles; gold nanocomposites; layer-by-layer assembly; neural stimulation; implantable devices; inflammation; microfabrication

INTRODUCTION

Neural prosthetic devices (NPDs), like artificial pacemakers[1] and cochlear implants[2] are becoming increasingly relevant for the diagnosis and treatments of many neurological conditions and traumas. Commonly, these devices utilize electrodes to interact with neural tissues and achieve targeted stimulation or recording. For example, chronic deep brain stimulation (DBS) can alleviate symptoms of Parkinson’s[3] and even Alzheimer’s disease.[4] NPDs have also allowed patients of ayomyotrophic lateral sclerosis to regain motor functions.[5] Recently, brain-computer interfaces have received increased attention due to the possibility of using multi-site recording NPD platforms for restoration of mobility and prosthetic devices for limbs.[6, 7] Despite initial clinical successes, there are still many challenges in creating long-lasting, high-performance neural prosthetic devices.

To improve the long-term stability and performance of current NPDs, it is necessary to minimize the inflammatory response induced by NPDs. Typically, after implantation, a layer of scar tissue forms around the NPD due to accumulation of resident immune cells.[8, 9] This layer will create a barrier between the device and the target neural tissue, which causes the device to lose its functionality overtime.[10]

*To whom correspondence should be addressed: kotov@umich.edu.

SUPPORTING INFORMATION AVAILABLE:
Additional figures (Figures S1–S6). This material is available free of charge via the Internet at http://pubs.acs.org.

Studies have suggested that inflammatory response is substantially reduced as the implant becomes smaller.[11, 12] The ideal dimensions of implantable neural electrodes should not exceed 10 μm in either width or thickness.[13] Moreover, it was demonstrated that subcellular-sized electrodes allow the formation of tight junction between neurons and electrodes, thus creating effective electrical coupling at the neuron/electrode interface.[14] Mechanical properties of the electrodes are also closely related to inflammation. Electrodes made of rigid materials, such as noble metals and semiconductors have large mismatches in mechanical properties with neural tissues.[15, 16] This mismatch becomes particularly significant when considering the inevitable microscale motion of electrodes relative to the brain tissues.[17] This motion triggers additional immune response through mechanical signal transduction.[12] Smaller flexible electrodes have better compliance with soft tissues and are expected to help reduce the additional activation of immune reactions and scar formation.

While the concept of ultrasmall flexible electrodes is well understood, the pathway to its practical realization is not. The ultrasmall electrodes bring up challenging material issues. The electrical properties of all current classical and advanced materials exemplified by platinum, doped silicon, polypyrrole, poly(3,4-ethylenedioxythiophene)(PEDOT), and iridium oxide (IrOx), greatly limit the functionalities of electrodes smaller than 50–100 μm. The charge storage capacity (CSC) and interfacial impedance (Z) of these materials are not sufficient to reliably record signals from electrodes below this size.

To resolve these issues, it is necessary to develop new materials with improved Z and CSC than current materials.[18] Lower electrical impedance improves signal-to-noise ratio and the long-term recording quality of NPDs[19, 20] and reduces harmful overpotential. High CSC materials can deliver a higher charge per area of the electrodes to the surrounding tissue for neural stimulation. The general strategy for improving Z and CSC is to increase the electrochemical surface area of the electrodes for a given geometric surface area.[21, 22] Most advanced materials used for neural electrodes, including platinum black,[23] conductive polymer,[24] and iridium oxide[25] have high-roughness surfaces to increase the ratio of electrochemical surface area and geometric surface area, consequently improving the Z and CSC. Evidently, conductive nanomaterials would be ideal for engineering the surfaces of the neural electrodes.

Currently, most research on nanomaterials for neural interface is mainly focused on CNT-based material.[20, 26–36] It has been demonstrated that CNT coating improves *in vivo* neural recording both in rats and primates.[20] Despit*e* excellent mechanical properties of CNT, the electrochemical performance of CNT composites is still not as high as needed for the ultrasmall NPD devices with dimensions ≤10μm.

Biocompatibility and related inflammation processes initiated by electrodes from CNT or other materials with respect to long-term implantation (on the scale of years) remains a concern[37] that needs to be addressed in the future. These challenges drive us to explore other nanomaterials and further optimize the electrochemical properties of neural interface materials.[38, 39] Additionally, nanoporous gold and gold nanopowder were also investigated for neural interface applications.[22, 40] Both studies demonstrated the possibility of creating high roughness gold surfaces. However, these techniques require extensive instrumentation (ultra high vacuum deposition and mold fabrication) and high processing temperatures.

Solution processed gold nanoparticles (Au NPs) have been studied extensively for their biological applications.[41] They have minimal toxicity,[42] are highly conductive,[43] and are very simple to fabricate.[44] Au NP/polymer composites have great potential for NPD

application in term of electrochemical performance and biocompatibility, but Au NPs have never been used for neural interface applications. A lot of attention paid to carbon nanotubes (CNT) probably overshadowed gold NPs as material suitable for neural interface. CNTs were considered *a priori* to be a better choice due to their fibrous morphology, high electron mobility, and high surface area. [26] Here we demonstrate that this assumption was probbaly incorrect and materials with better electrochemical performance can be made from Au NPs. Measurements of electrochemical properties on NPD prototypes indicate that in respect to Z and CSC, Au NP films substantially outperform SWNT composites. Since the microfabrication process developed here for Au NP composites is compatible with current microelectrode technology, this study opens the way to a new generation of implantable electrodes.

RESULTS AND DISCUSSION

Previous comparative evaluation of IrOx and PEDOT with CNT composite concluded that CNT composite outperform IrOx and PEDOT with respect to both electrical and mechanical properties upon cyclic excitation.[26] The major effort here is to answer the question of whether materials even better than CNT composite could be created. Au NPs attracted our attention because the conductivity of macroscale composite materials made from Au NPs is higher than any other CNT composites thus far.[45, 46] The charge transport in a single carbon nanotube can be exceptionally fast, but this does not mean that it is possible to translate it to macroscale materials. Unfortunately, the insulating gaps between the nanotubes and the Schottky barrier at the interfaces between the semiconductor and metallic nanotubes greatly frustrate the electron transport in CNT materials in macro- and microscale. [47] Further improvements in CNT synthesis could potentially resolve some of these issues. At the same time, these prompted us to explore alternatives presented by other nanomaterials exemplified by Au NPs. Besides high conductivity of macroscale composites, Au NPs provide exceptionally high surface area, which can potentially reduce Z. The challenge in this case will be to balance the surface area with the interconnectivity of NPs.

Latest results indicated that carbon nanostructures could undergo biodegradability upon long-term exposure to biological media,[48] which could present a problem for NPD applications. According to existing data,[49] Au NPs at a certain level do not interfere with tissue function even after many years of residence time, which is a substantial advantage for NPD implants.

For valid comparison between CNTs and Au NPs, the same technique of film preparation is needed. The universality of the layer-by-layer (LBL) assembly offers this possibility. Compare to some other methods of thin film deposition, such as electrophoresis, chemical vapor, and solvent evaporation,[50] LBL requires milder operating conditions, simpler instrumentations, and most importantly, provides a higher degree of structural control. It also allows one to combine organic and inorganic materials, which is necessary for biomedical applications. Last, but not the least, LBL makes it possible to accurately control the thickness of the coatings by controlling the number of deposition cycles, n. This is particularly important for the adequate comparison between Au NP and CNT film. By and large, LBL can be depicted as a versatile method to engineer multifunctional coatings down to the nanometer scale[51] and to fine tune the entire spectrum of materials properties: mechanical, electrical, optical, and biological to achieve the balanced combination specific for the particular application.[52–54]

Therefore, LBL assembly was applied for the preparation of Au NP and SWNT composite thin films on electrodes. SWNT LBL films were assembled from SWNT aqueous dispersions stabilized by poly(styrene sulfonate) (PSS) using poly(vinyl alcohol) as a partner

LBL polymer following the protocol described in our previous study and the method section.[46, 55] Au NP LBL films were made using concentrated citrate-stabilized NPs in water. In this case, we used standard polymer, poly(diallydimethylammonium chloride) (PDDA) as an LBL-partner, which was used in many previous LBL applications.[56] We specifically selected for this project the polymers that are electrochemically "silent" in the window of potential relevant for neural stimulation. Besides making it easier to understand the electrochemical performance of the coatings (see below), having electrochemically inactive polymers as partners for NPs and CNTs is important in order to avoid their redox decomposition, which is certainly undesirable.

From atomic force microscopy (AFM) images and ellipsometry data (Figure 1), one can establish that Au NPs and CNT LBL films can be successfully deposited in the sequential manner despite a complex film growth curve (Figure 1D). The NP LBL film displays a rough surface with close packed Au NPs. The surface morphology of the Au NP films can be described as globular while the CNT films are fibrous with random orientation of the nanotubes within X–Y plane. Both nanoscale morphologies are important for increasing electrochemical surface area and improving the NPD performance. Scanning electron microscopy (SEM) images of Au NP and SWNT films also exhibit similar geometrical features (Figure 2).

The total number of LBL deposition cycles was adjusted for both nanomaterials to obtain the same coating thickness. Cross-sectional SEM images for CNT and Au NP films obtained after 25 and 15 deposition cycles respectively show a thickness of 100±8 nm. The same image also indicates high content and interconnectivity of Au NP in the films.

We first compared the performance of the CNT coating in our study with the previous study. The same wire electrode were fabricated and tested under the identical conditions to those previous ones. The impedance of our CNT coating is about 170Ω compare to previously reported 277Ω at the physically relevant frequency. And the CSCs of the two coatings are also very similar, approximately 10mC/cm^2.

To further ensure accurate electrochemical measurements, we designed a lithographic scheme to integrate LBL nanocomposite films into the microelectrode fabrication process (Figure 3). The electrode design guarantees that all films tested have the same surface area and their geometry is perfectly reproducible from batch to batch. The chosen microfabrication process (Figure 3) allows minimal exposure of the nanocomposite films to other process chemicals. EDAX spectroscopy indicates that the nanocomposite films are unaltered after the microfabrication process and that there are no residual chemicals on the surfaces of the films (Supplemental Information). Besides its convenience and accuracy, the design of these microelectrodes can be adapted to virtually any type of implants including those with dimensions of 10 μ and less.

Impedance (Z) and charge storage capacity (CSC) were investigated in a three-electrode electrochemical set-up, which is most suitable for the measurement of these properties. Impedance was measured by a frequency response analyzer from 10 Hz to 31 kHz. Au NP film has lower Z than SWNT film for the entire spectrum of frequencies relevant for NPDs. The characteristic impedance phase angles (Φ) for Au NP film across the entire frequency domain are smaller than SWNT film, which implies the higher conductivity of Au NP film (Figure 4A, B). This is further confirmed by the conductivity measurements in an ambient environment with a standard four-point probe. The conductivity of Au NP film is 8.6*10^6 S/m; this is more than a magnitude higher than conductivity of CNT film equal, 1.1*10^5 S/m. [57] The area enclosed in the CV curve, S, of Au NP film is much larger than SWNT film for the same scan rate, v, indicating a substantially higher CSC.

Detailed comparison of Au NP and CNT film are made by using impedance values measured for 1 kHz and cathodic CSC. In Figures 4D and 4F, the average measurements of 32 samples indicate that Au NP film outperform SWNT film with respect to both *Z* and cathodic *CSC*. P-values for Z and CSC were less than 0.01 for a two-tail Student t-test, indicating that the differences between CNT and Au NP film are statically significant. The *Z* value of Au NP film is almost four times lower than SWNT film while the cathodic *CSC* of the Au NP film is close to one magnitude higher than SWNT film.

Total CSC is also quite informative although it is somewhat more difficult to compare. Previously, the total CSC of electrodes made from multiwalled carbon nanotubes, PEDOT, and IrO have been reported. The total CSC of these materials for 100 nm thick coatings and a scan rate of 0.1 V/s from −0.9V to 0.5 V ranged from 6 to 9 mC/cm^2.[27] In our study, the total CSC of the 100nm thick Au NP films at a scan rate of 1 V/s from −0.6V to 0.8V was 2.56 mC/cm^2 (Figure 4D). The actual voltage window is determined by the specific redox properties of the material and can be rarely matched exactly. The effect of the scan rate can be incorporated as a scaling factor because CSC is inversely proportional to the scan rate. Note that the width of the voltage window was, nevertheless, identical in each case and equal to 1.4V. Recalculating the literature data to a 1 V/s scan rate scale shows that the total CSC for Au NP film is at least three times higher than analogous data in the previous report. [27]

Besides determining CSC, CV experiments also offer additional information at the electrode/electrolyte interface. We noticed a reduction peak in the CV curve of Au NP film. In order to identify this reduction peak, we conducted a control CV experiment with argon gas purged PBS solution instead of regular PBS solution. The reduction peak disappeared after the argon purge of the PBS solution. This indicates that the peak is from the reduction of oxygen (See Supplemental Information). observed on many metal electrodes, including gold electrodes. [40]

Furthermore, we also conducted voltage transient experiments to evaluate the performance of Au NP film and CNT film. This technique is commonly used to determine the charge injection limit of an electrode for a given voltage limit.[21] Cathodic current pulse (−5μA, 2ms) was applied to the electrodes while the voltage was recorded. For the same amount of charge, Au NP film has a lower voltage excursion compared to CNT film (Figure 4F). This indicates that Au NP film has a high charge injection limit compared to CNT film for a given voltage limit. This result correlates well with the impedance data because lower impedance generally reduces overpotential and lowers the voltage excursion.

The circuit analogs of impedance data can be used to gain detailed insight about the materials properties and interfacial properties of an NPD. The circuit analog used here (Figure 5A) assumed the measured impedance was a product of electrical resistance of the film (R_s), charge transport losses at the film-electrolyte interface (R_f), and interfacial capacitance of the film (C_d). Walburg impedance (*W*) was previously included in many analog circuits as well. However, *W* is only relevant for systems with strong mass transport limitations. For the operating environment of NPDs, one can consider that the transport limitations to be minimal due to the large amount of ions present and the small amount of charge transferred. By fitting the impedance data using this circuit analog (Figure 5A), the experimental impedance *Z* is lower for Au NP film (Figures 4A, D) due to the lower R_s, and R_f. The high *CSC* values for Au NP films can be correlated with high value of C_d. This indicates that the high surface area created by NPs and the high interconnectivity among NPs in the composite materials play essential roles in determining the macroscale electrochemical functionalities. It might be important to note that *CSC* of solid noble films is typically low. Platinum/Iridium alloy which is the best choice for metallic neural electrode,

only has a theoretical maximum *CSC* of 0.3 mC/cm^2, [21] and the *CSC* of pure metallic Au is even lower. The marginal *CSC* of noble metals prevents the possibility of fabricating high performance stimulating microelectrodes from the classical evaporation+microfabrication techniques.

To further evaluate the feasibility of Au NP LBL film for neural interface applications, we conducted electrochemical stability tests for both Au NP and SWNT LBL films. In part, it was also important for comparative purposes because SWNT films are known for their remarkable environmental resilience. Therefore, both films were subjected to a 500 CV scanning cycle at a fast scan rate of 1 V/s. As illustrated in Figure 4E, the *CSC* of both films decreases initially, then stabilizes around 400 cycles. This demonstrates that Au LBL films offer similar stability compared to SWNT films, which is quite remarkable considering the exceptional mechanical properties of individual CNTs and the fact that they have virtually perfect planar orientation in LBL films (Figure 1D), which provides the best translation of their mechanical properties to the composites.

Besides excellent electrochemical properties, neuron adhesion/surface biocompatibility is also very important for high quality *in vivo* recording. A close interface between electrode/neuron improves the quality of the recording.[14, 20] The biocompatibility of the Au NP/PDDA coating was tested with *in-vitro* culture of NG108-15 cells, a type of mouse neuroblastoma/glioma hybrid cells, which are typically used in many biocompatibility/toxicity protocols[58]. Cells were seeded and cultured on glass slides coated with Au NP/PDDA film. Optical images showed NG108 cells could adhere well on the coating and differentiate into neuron-like morphology. (See Supplemental Information) Live/Dead assay were also performed and indicated that 99.9% of cells were live on the surface of the Au NP/PDDA coating (Figure 5B). Additionally, the mechanical integrity of Au NP film was also examined by an *ex-vivo* insertion test. The electrodes coated with Au NP/PDDA were inserted into a fresh harvested rat brain and kept at 4°C for 3 days. Then the electrodes were removed from the brain, rinsed with PBS, and imaged with SEM. The Au NP/PDDA coating surface retains the same nanoscale roughness as observed before the insertion (Figure 5C,D).

CONCLUSIONS

Quite unexpectedly, Au NP films were found to have remarkable charge transfer capacity, substantially lower impedance and comparable electrochemical stability under fast voltage scans than CNT films made using the same technology, which were previously considered to be the most promising new materials for the next generation of implantable neuroprosthetic devices (NPDs). Besides the electrochemical performance, we also see additional advantages of the described Au NP films with respect to other (nano)materials: (1) the long-standing clinical record of gold in both nano- and macroscale forms will facilitate their acceptance; (2) LBL assembly offers tremendous possibilities for further optimization and adaptation to additional NPD functions, which for instance can include *in-situ* gene delivery.[59] Further improvement of materials performance is also possible using LBL films from novel Au NPs, such as nanoshells and nanostars.

A general microfabrication process for Au NP LBL composites suitable for preparation of ultrasmall implantable electrodes that can be virtually “invisible” to the immune system was designed and realized. Integration of LBL film deposition technology and traditional lithography opens many possibilities for utilization of nanostructured LBL composites from CNTs, NPs, etc and their unique properties in many applications.

Further optimization at the system level combining the material properties of Au NP composites and microfabrication techniques must also be pursued. Fabrication of electrodes, which are mechanically compliant with the soft neural tissues and *in vivo* evaluation of this type of microelectrodes, should be the next logical step in this field. A flexible and high performance electrode made out of Au NP film could minimize the tissue stress and provide long-term stability for future neural prosthetic devices.

MATERIALS AND METHODS

High purity single wall carbon nanotubes (P2-SWNTs) were purchased from Carbon Solution, Inc. (Riverside, CA), respectively. Poly(vinyl alcohol) (PVA; MW 70k), poly(sodium 4-styrene-sulfonate) (PSS; MW 100k), and Poly(diallyldimethylammonium chloride) (PDDA)were obtained from Sigma-Aldrich. All other chemicals were obtained from Sigma-Aldrich

Synthesis of Gold Nanoparticles followed the standard citrate reduction method. Briefly, 90 mg of HAuCl4 were dissolved in 500 ml of water. The solution was heated on a hot plate until boiling. Then 25ml of 0.1% sodium citrate aqueous solution was added to the gold salt solution. The mixture was stirred and reboiled on a hot plate. After 20 minutes, the solution would become a red color, which indicated the formation of gold nanoparticles. The gold nanoparticles were concentrated 10X by centrifuging at 9000 rpm for 50 minute and removing 90% of the supernatant.

Layer-by-Layer Assembly of Au NP film and SWNT film was initially carried out on microscope glass slides cleaned in piranha solution overnight and then thoroughly rinsed with deionized water prior to the use. For LBL assembly, a glass slide was immersed in 0.1 wt % solution of PDDA for 5 min, rinsed with DI water for 1 min, dried, and then immersed in concentrated Au NP solution for 10 min, rinsed for 1 min, and dried again. The procedure was then repeated with PDDA and Au NP solution.

SWNTs were first dispersed at 0.5 mg/mL in 2mg/ml PSS (MW 100k) solution by ultrasonication. 0.1 wt % PVA solution was prepared by dissolving correct amount of PVA in near boiling water. For each deposition cycle, the electrode was immersed in the PVA solution for 2 min, following by rinsing with deionized water and drying with an air jet. Then the electrode was immersed in SWNT solution for 5 min, following by rinsing with deionized water and drying with an air jet.

Fabrication of LBL Coated Electrode involved several standard microfabrication procedures. Briefly, positive photoresist (SPR-220 3.0, Rohm and Haas) was first deposited and developed on a glass slide. Then 500nm of metallic gold were deposited by electron beam (Enerjet Evaporator, Denton) at a base pressure of 2*10^−6 torr onto the photoresist coated glass slides. After evaporation, gold were lifted off from the glass in acetone to form the electrode layer. The same positive photoresist were deposited again and developed to form lift-off layer for the LBL film. Afterward, LBL assembly process was applied to the electrode. Once the LBL film achieved the target thickness, the glass slide was transferred in acetone for LBL film lift-off. Lastly, the final layer of positive photoresist was deposited and developed as an insulation layer.

Electrochemical Impedance Spectroscopy (EIS) was carried out on an Autolab PGSTAT 12; Frequency Response Analyzer software (EcoChemie, Utrecht, Netherlands) was used to record impedance spectra of the electrodes. A solution of 1 M phosphate buffered saline (PBS, pH = 7) was used as an electrolyte in a three-electrode configuration. The working electrode was connected to the electrode site. The counter electrode was connected to a gold

foil immersed in PBS, and an Ag/AgCl reference electrode was immersed in PBS. An AC sinusoidal signal of 25 mV in amplitude was used to record the impedance over a frequency range of 10–32000 Hz.

Cyclic Voltammetry (CV) and Voltage Transients experiments were performed using an Autolab PGSTAT 12 instrument and General Purpose Electrochemical System software (EcoChemie, Utrecht, Netherlands) in a three-electrode configuration as described for EIS. For CV, a scan rate of 1 V/s was used and the potential on the working electrode was swept between −0.8 and 0.6 V. Three cycles were swept to ensure that the film had reached a stable state. For the voltage transient experiment, a cathodic current pulse (5μA, 2ms) were sourced and voltage change were recording during the experiment.

NG108-15 Cell Culture and Biocompatibility Test: NG108-15 cell line was obtained from American Type Culture Collection (ATCC: HB 12317). The cells were culture with DMEM high glucose media (Gibco: 11965-092) + Hypoxanthine − Aminopterin − Thymidine supplement (ATCC: 69-X) +10% fetal bovine serum at 37°C with 5% CO_2. Once the cells reached 90% confluence, they were detached from the culture flask and 1*10^6 cells were seeded onto a 1cm by 1 cm glass slide coated with Au NP/PDDA film. The cells were culture in the same condition for three days on the glass slide before the biocompatibility test. The biocompatibility of the Au NP/PDDA films was tested by a LIVE/DEAD Biohazard Cell Viability Kit (Invitrogen: L-7013) according to the exact protocol provided the vendor. Then the live and dead cells were counted and cell viability was calculated by dividing the number of live cells by the total number of the cell on the substrate.

Scanning Electron Microscopy (SEM) images were obtained using a FEI Nova Nanolab SEM at 10kV accelerating voltage.

Atomic Force Microscopy (AFM) images were obtained using Digital Instrument Nanoscope (R) at a scan rate of 0.5 Hz and tip speed of 30 μm/s.

Transmition Electron Microscopy (TEM) images were obtained using a JEOL 3010 TEM with acceleration voltage of 300kV.

Supplementary Material

Refer to Web version on PubMed Central for supplementary material.

Acknowledgments

We acknowledge support from NSF under grant ECS-0601345; EFRI-BSBA 0938019; CBET 0933384; CBET 0932823; and CBET 1036672. The work is also partially supported by AFOSR MURI 444286-P061716 and NIH 1R21CA121841-01A2. This material is based upon work partially supported by the Center for Solar and Thermal Energy Conversion, an Energy Frontier Research Center funded by the U.S. Department of Energy, Office of Science, Office of Basic Energy Sciences under Award Number #DE-SC0000957. The authors thank the University of Michigan's EMAL for its assistance with electron microscopy and for the NSF grant #DMR-9871177, Leslie George, Edward Tang from the University of Michigan Lurie Nanofabrication Facility for assistance with microfabrication techniques. The authors also thank Paras Patel (Biomedical Engineering, UM), Dr. Edward Jan (3D Biomatrix LLC), Dr. Takashi D. Yoshida Kozai (Biomedical Engineering, UM), Prof. Daryl R. Kipke (Biomedical Engineering, UM) and Prof. Eusik Yoon (Electrical and Computer Engineering, UM) for assistance and helpful discussion on electrochemical methods and neural electrodes. The authors also thank Dr. Matthew Di Prima (Chemical Engineering, UM) for helpful discussion on layer-by-layer techniques.

References

1. Callaghan JC, Bigelow WG. An electrical artificial pacemaker for standstill of the heart. Annals of surgery. 1951; 134(1):8–17. [PubMed: 14838536]

2. Fallon JB, Irvine DR, Shepherd RK. Cochlear implants and brain plasticity. Hear Res. 2008; 238(1–2):110–7. [PubMed: 17910997]
3. Pena C, Bowsher K, Samuels-Reid J. FDA-approved neurologic devices intended for use in infants, children, and adolescents. Neurology. 2004; 63(7):1163–1167. [PubMed: 15477532]
4. Hamani C, et al. Memory enhancement induced by hypothalamic/fornix deep brain stimulation. Annals of neurology. 2008; 63(1):119–23. [PubMed: 18232017]
5. Nijboer F, et al. A P300-based brain-computer interface for people with amyotrophic lateral sclerosis. Clinical neurophysiology: official journal of the International Federation of Clinical Neurophysiology. 2008; 119(8):1909–16. [PubMed: 18571984]
6. Velliste M, et al. Cortical control of a prosthetic arm for self-feeding. Nature. 2008; 453(7198): 1098–101. [PubMed: 18509337]
7. Moritz CT, Perlmutter SI, Fetz EE. Direct control of paralysed muscles by cortical neurons. Nature. 2008; 456(7222):639–42. [PubMed: 18923392]
8. Biran R, Martin DC, Tresco PA. Neuronal cell loss accompanies the brain tissue response to chronically implanted silicon microelectrode arrays. Experimental neurology. 2005; 195(1):115–26. [PubMed: 16045910]
9. Edell DJ, et al. Factors influencing the biocompatibility of insertable silicon microshafts in cerebral cortex. IEEE transactions on bio-medical engineering. 1992; 39(6):635–43. [PubMed: 1601445]
10. Davies SJ, et al. Regeneration of adult axons in white matter tracts of the central nervous system. Nature. 1997; 390(6661):680–3. [PubMed: 9414159]
11. Kim YT, et al. Chronic response of adult rat brain tissue to implants anchored to the skull. Biomaterials. 2004; 25(12):2229–37. [PubMed: 14741588]
12. Keohan F, et al. Fabrication and evaluation of conductive elastomer electrodes for neural stimulation. Journal of biomaterials science Polymer edition. 2007; 18(8):1057–73. [PubMed: 17705998]
13. Sanders JE, Stiles CE, Hayes CL. Tissue response to single-polymer fibers of varying diameters: evaluation of fibrous encapsulation and macrophage density. Journal of biomedical materials research. 2000; 52(1):231–7. [PubMed: 10906696]
14. Hai A, Shappir J, Spira ME. In-cell recordings by extracellular microelectrodes. Nature methods. 2010; 7(3):200–2. [PubMed: 20118930]
15. Subbaroyan J, Martin DC, Kipke DR. A finite-element model of the mechanical effects of implantable microelectrodes in the cerebral cortex. Journal of neural engineering. 2005; 2(4):103–13. [PubMed: 16317234]
16. Seymour JP, Kipke DR. Neural probe design for reduced tissue encapsulation in CNS. Biomaterials. 2007; 28(25):3594–607. [PubMed: 17517431]
17. Gilletti A, Muthuswamy J. Brain micromotion around implants in the rodent somatosensory cortex. Journal of neural engineering. 2006; 3(3):189–95. [PubMed: 16921202]
18. Merrill DR, Bikson M, Jefferys JG. Electrical stimulation of excitable tissue: design of efficacious and safe protocols. J Neurosci Methods. 2005; 141(2):171–98. [PubMed: 15661300]
19. Harnack D, et al. The effects of electrode material, charge density and stimulation duration on the safety of high-frequency stimulation of the subthalamic nucleus in rats. J Neurosci Methods. 2004; 138(1–2):207–16. [PubMed: 15325129]
20. Keefer EW, et al. Carbon nanotube coating improves neuronal recordings. Nature nanotechnology. 2008; 3(7):434–9.
21. Cogan SF. Neural stimulation and recording electrodes. Annu Rev Biomed Eng. 2008; 10:275–309. [PubMed: 18429704]
22. Seker E, et al. The fabrication of low-impedance nanoporous gold multiple-electrode arrays for neural electrophysiology studies. Nanotechnology. 2010; 21(12):125504. [PubMed: 20203356]
23. Marrese CA. Preparation of Strongly Adherent Platinum Black Coatings. Analytical Chemistry. 1987; 59(1):217–218.
24. Richardson-Burns SM, et al. Polymerization of the conducting polymer poly(3,4-ethylenedioxythiophene) (PEDOT) around living neural cells. Biomaterials. 2007; 28(8):1539–52. [PubMed: 17169420]

25. Blau A, et al. Characterization and optimization of microelectrode arrays for in vivo nerve signal recording and stimulation. Biosensors & bioelectronics. 1997; 12(9–10):883–92. [PubMed: 9451781]
26. Jan E, et al. Layered Carbon Nanotube-Polyelectrolyte Electrodes Outperform Traditional Neural Interface Materials. Nano Letters. 2009; 9(12):4012–4018. [PubMed: 19785391]
27. Jan E, Kotov NA. Successful differentiation of mouse neural stem cells on layer-by-layer assembled single-walled carbon nanotube composite. Nano Letters. 2007; 7(5):1123–1128. [PubMed: 17451277]
28. Kam NWS, Jan E, Kotov NA. Electrical Stimulation of Neural Stem Cells Mediated by Humanized Carbon Nanotube Composite Made with Extracellular Matrix Protein. Nano Letters. 2009; 9(1):273–278. [PubMed: 19105649]
29. Gheith MK, et al. Single-walled carbon nanotube polyelectrolyte multilayers and freestanding films as a biocompatible platformfor neuroprosthetic implants. Advanced Materials. 2005; 17(22): 2663.
30. Luo X, et al. Highly stable carbon nanotube doped poly(3,4-ethylenedioxythiophene) for chronic neural stimulation. Biomaterials. 2011; 32(24):5551–7. [PubMed: 21601278]
31. Lovat V, et al. Carbon nanotube substrates boost neuronal electrical signaling. Nano Letters. 2005; 5(6):1107–1110. [PubMed: 15943451]
32. Malarkey EB, et al. Conductive Single-Walled Carbon Nanotube Substrates Modulate Neuronal Growth. Nano Letters. 2009; 9(1):264–268. [PubMed: 19143503]
33. Cellot G, et al. Carbon nanotubes might improve neuronal performance by favouring electrical shortcuts. Nature nanotechnology. 2009; 4(2):126–133.
34. Malarkey EB, Parpura V. Carbon Nanotubes in Neuroscience. Brain Edema Xiv. 2010; 106:337–341.
35. Luo XL, et al. Highly stable carbon nanotube doped poly(3,4-ethylenedioxythiophene) for chronic neural stimulation. Biomaterials. 2011; 32(24):5551–5557. [PubMed: 21601278]
36. Wang K, et al. Neural stimulation with a carbon nanotube microelectrode array. Nano Letters. 2006; 6(9):2043–2048. [PubMed: 16968023]
37. Firme CP 3rd, Bandaru PR. Toxicity issues in the application of carbon nanotubes to biological systems. Nanomedicine: nanotechnology, biology, and medicine. 2010; 6(2):245–56.
38. Cohen-Karni T, et al. Graphene and Nanowire Transistors for Cellular Interfaces and Electrical Recording. Nano Letters. 2010; 10(3):1098–1102. [PubMed: 20136098]
39. Qing Q, et al. Nanowire transistor arrays for mapping neural circuits in acute brain slices. Proceedings of the National Academy of Sciences of the United States of America. 2010; 107(5): 1882–1887. [PubMed: 20133836]
40. Hu Z, et al. Nanopowder molding method for creating implantable high-aspect-ratio electrodes on thin flexible substrates. Biomaterials. 2006; 27(9):2009–17. [PubMed: 16310844]
41. Sperling RA, et al. Biological applications of gold nanoparticles. Chemical Society reviews. 2008; 37(9):1896–908. [PubMed: 18762838]
42. Zhang XD, et al. Toxicologic effects of gold nanoparticles in vivo by different administration routes. International journal of nanomedicine. 2010; 5:771–81. [PubMed: 21042423]
43. Critchley K, et al. Near-bulk conductivity of gold nanowires as nanoscale interconnects and the role of atomically smooth interface. Advanced Materials. 2010; 22(21):2338–42. [PubMed: 20376858]
44. Turkevich J, Stevenson PC, Hillier J. A Study of the Nucleation and Growth Processes in the Synthesis of Colloidal Gold. Discussions of the Faraday Society. 1951; (11):55.
45. Liu YJ, Wang YX, Claus RO. Layer-by-layer ionic self-assembly of Au colloids into multilayer thin-films with bulk metal conductivity. Chemical Physics Letters. 1998; 298(4–6):315–319.
46. Shim BS, et al. Multiparameter Structural Optimization of Single-Walled Carbon Nanotube Composites: Toward Record Strength, Stiffness, and Toughness. Acs Nano. 2009; 3(7):1711–1722. [PubMed: 19591447]
47. Odintsov AA. Schottky barriers in carbon nanotube heterojunctions. Physical Review Letters. 2000; 85(1):150–153. [PubMed: 10991181]

48. Kagan VE, et al. Carbon nanotubes degraded by neutrophil myeloperoxidase induce less pulmonary inflammation. Nature nanotechnology. 2010; 5(5):354–359.

49. Thakor AS, et al. Gold Nanoparticles: A Revival in Precious Metal Administration to Patients. Nano Letters. 2011; 11(10):4029–4036. [PubMed: 21846107]

50. Kotov NA, et al. Nanomaterials for Neural Interfaces. Advanced Materials. 2009; 21(40):3970–4004.

51. Srivastava S, Kotov NA. Composite Layer-by-Layer (LBL) assembly with inorganic nanoparticles and nanowires. Accounts of chemical research. 2008; 41(12):1831–41. [PubMed: 19053241]

52. Shim BS, et al. Multiparameter structural optimization of single-walled carbon nanotube composites: toward record strength, stiffness, and toughness. Acs Nano. 2009; 3(7):1711–22. [PubMed: 19591447]

53. Zhu J, et al. Transparent conductors from carbon nanotubes LBL-assembled with polymer dopant with pi-pi electron transfer. Journal of the American Chemical Society. 2011; 133(19):7450–60. [PubMed: 21524068]

54. Shim BS, et al. Transparent conductors from layer-by-layer assembled SWNT films: importance of mechanical properties and a new figure of merit. Acs Nano. 2010; 4(7):3725–34. [PubMed: 20552974]

55. Shim BS, et al. Integration of conductivity transparency, and mechanical strength into highly homogeneous layer-by-layer composites of single-walled carbon nanotubes for optoelectronics. Chemistry of Materials. 2007; 19(23):5467–5474.

56. Sinani VA, et al. Collagen coating promotes biocompatibility of semiconductor nanoparticles in stratified LBL films. Nano Letters. 2003; 3(9):1177–1182.

57. Zhu J, et al. Transparent Conductors from Carbon Nanotubes LBL-Assembled with Polymer Dopant with pi-pi Electron Transfer. Journal of the American Chemical Society. 2011; 133(19): 7450–7460. [PubMed: 21524068]

58. Adler M, et al. Cytotoxic actions of the heavy metal chelator TPEN on NG108-15 neuroblastoma-glioma cells. Neurotoxicology. 1999; 20(4):571–82. [PubMed: 10499356]

59. Jan E, et al. In situ gene transfection and neuronal programming on electroconductive nanocomposite to reduce inflammatory response. Journal of Materials Chemistry. 2011; 21(4): 1109–1114.

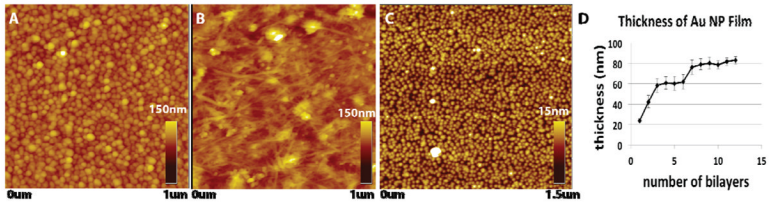

Figure 1.

(A) AFM image of 15 bilayers of Au NP LBL film. (B) AFM image of 25 bilayers of CNT LBL film. (C) First bilayer of Au NP LBL film. (D) Ellipsometric thickness of Au NP LBL films for different number of bilayers.

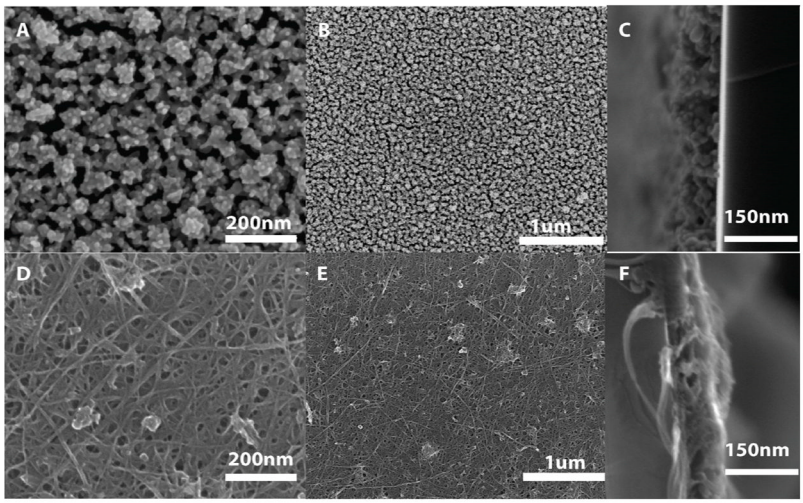

Figure 2.
SEM images of Au NP film and CNT film. (A, B) SEM images of Au NP film at different magnifications. (C) Cross-section image of Au NP film. (D, E) SEM images of CNT film at different magnifications. (F) Cross-section image of CNT film.

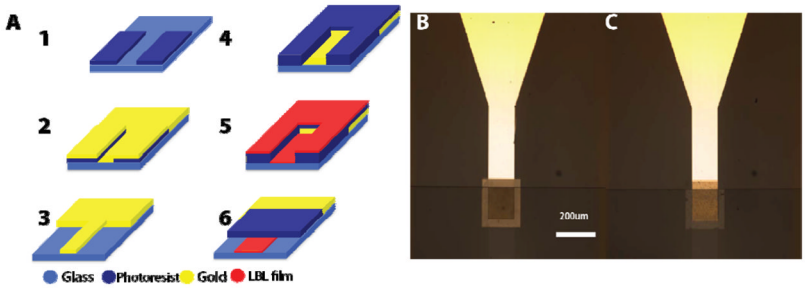

Figure 3.

(A) Fabrication process of the microelectrodes with LBL films of Au NPs and CNTs (1) deposition and development of the positive photoresist; (2) E-beam deposition of the metal gold; (3) lift-off of the metal gold layer; (4) deposition and development of the positive photoresist (5) depo-sition of the LBL film (6) lift-off of LBL film and deposition/ development of insulating photo-resist layer. (B) Optical image of Au NP LBL film coated electrode. (C) Optical image of CNT LBL film coated electrode.

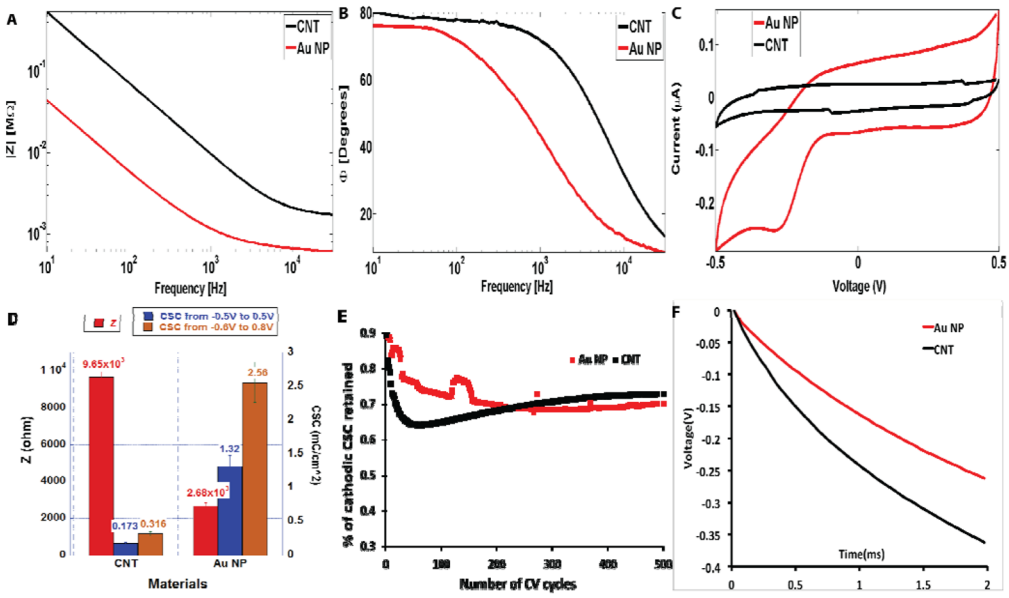

Figure 4.

Typical electrochemical behavior of Au NP film (red) and CNT films (black): (A) Frequency dependence of impedance, Z. (B) Frequency dependence of the impedance phase angle, Φ; (C) Typical cyclic voltammetry from 0.5 V to −0.5 V. (D) Cumulative electrochemical properties of Au NP and CNT films. The data were calculated for sample size of 32 samples. (E) Evaluation of stability of Au NP and CNT films over 500 CV cycles at 1 V/s scan rate for repeating electrochemical excitation. (F) Voltage transient experiment with cathodic current pulses (5μA, 2ms)

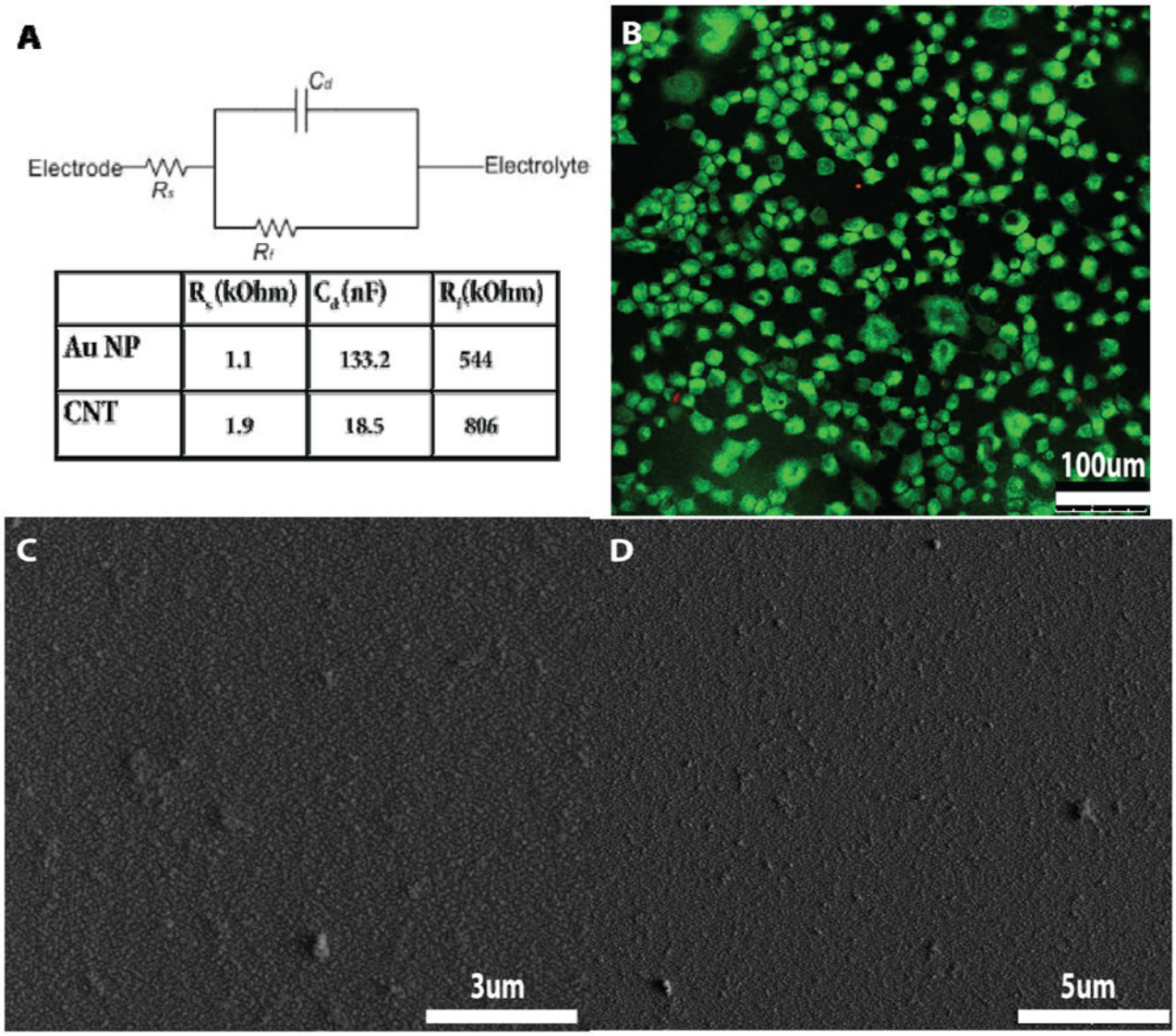

	R_s (kOhm)	C_d (nF)	R_f (kOhm)
Au NP	1.1	133.2	544
CNT	1.9	18.5	806

Figure 5.

(A) Circuit analog of the impedance data. (B) Sample confocal fluorescent image of LIVE/DEAD assay (Green:Live; Red:Dead). (C,D) SEM images of Au NP/PDDA LBL films before (C) and after (D) insertion into rat brain.